



HAL
open science

Fragile dense suspensions under shear rotation

Frédéric Blanc, François Peters, Jurriaan J J Gillissen, Michael E Cates,
Sandra Bosio, Camille Benarroche, Romain Mari

► **To cite this version:**

Frédéric Blanc, François Peters, Jurriaan J J Gillissen, Michael E Cates, Sandra Bosio, et al.. Fragile dense suspensions under shear rotation. 2022. hal-03837785v1

HAL Id: hal-03837785

<https://hal.science/hal-03837785v1>

Preprint submitted on 3 Nov 2022 (v1), last revised 10 Oct 2023 (v2)

HAL is a multi-disciplinary open access archive for the deposit and dissemination of scientific research documents, whether they are published or not. The documents may come from teaching and research institutions in France or abroad, or from public or private research centers.

L'archive ouverte pluridisciplinaire **HAL**, est destinée au dépôt et à la diffusion de documents scientifiques de niveau recherche, publiés ou non, émanant des établissements d'enseignement et de recherche français ou étrangers, des laboratoires publics ou privés.

Fragile dense suspensions under shear rotation

Frédéric Blanc,¹ François Peters,¹ Jurriaan J.J. Gillissen,² Michael E. Cates,³ Sandra Bosio,⁴ Camille Benarroche,⁴ and Romain Mari⁵

¹*Institut de Physique de Nice, CNRS UCA, Parc Valrose, 06108 Nice Cedex 2 France*

²*The Technology Partnership, Science Park, Melbourn, UK.*

³*DAMTP, Centre for Mathematical Sciences, University of Cambridge, Wilberforce Road, Cambridge CB3 0WA, UK*

⁴*Institut de Physique de Nice UMR7010, CNRS Université Côte d'Azur, Parc Valrose, 06108 Nice Cedex 2 France*

⁵*Université Grenoble Alpes & CNRS, LIPhy, 38000 Grenoble, France*

(Dated: November 3, 2022)

While quasi-Newtonian complex fluids under steady-state flow, dense non-Brownian suspensions exhibit complex “macro-fragile” behaviors under varying flow conditions, as revealed by abrupt shear inversions (reversals). Here, we introduce an experimental setup to systematically explore their macro-fragile response to shear rotations, where one suddenly rotates the principal axes of shear by an angle θ . This reveals a transient decrease of the shear stress under shear rotation. Moreover, the orthogonal shear stress, which vanishes in steady state, takes non-negligible values with a rich θ -dependence, changing qualitatively with ϕ , and resulting in a force that tends to reduce or enhance the direction of flow for small or large ϕ . These findings are confirmed and rationalized by particle-based numerical simulations and a recently proposed constitutive model. We show that the angular dependence of the orthogonal stress results from an interplay between hydrodynamic and contact stresses, which balance changes with ϕ .

Suspensions of non-Brownian hard particles in liquid form a large class of complex fluids [1, 2]. When solid and fluid are mixed in roughly equal proportion, they are called dense suspensions. Their widespread use in industry calls for the development of proper constitutive characterization and modelling, in order to enable reliable quantitative process design.

This effort has a long history [1]. In steady state, the viscosity of non-Brownian suspensions is observed to be either deformation-rate-independent [3, 4] or slightly shear thinning [5–9]. Shear thickening is also observed when particles are repulsive beyond pure hard-core forces [10, 11], but we here focus on the strictly hard-sphere case. The low shear-rate value of the viscosity increases with the solid volume fraction ϕ , and diverges at the jamming volume fraction ϕ_J [3, 4].

However, dense suspensions exhibit striking unsteady behaviors, e.g. the sharp viscosity drop in orthogonal superposition [12–15]. The simplest illustration is shear reversal, where a suspension initially sheared in steady state under a given deformation rate $\dot{\gamma}$, is suddenly sheared with a rate $-\dot{\gamma}$ [16]. The viscosity drops suddenly at reversal, passes through a minimum value and climbs up to its steady-state value after a few strain units [16–23].

Under shear, suspensions develop an anisotropic contact network which takes up most of the stress at large concentrations [10, 20, 24–29] and is built in a finite strain [16]. Upon shear reversal, the micro-structure is initially not compliant with the new direction of shear, leading to a viscosity dip which ends when the micro-structure is rebuilt in the new orientation [16]. The fact that the principal axes of the micro-structure have to rotate over a finite strain to sustain a change of

applied load is known as macrofragility [30]. For shear reversal, the rotation of the stress axes is maximal, as the compressional and elongational axes are swapped. The associated macro-fragile response has been carefully characterized numerically [21, 22, 31].

Beyond shear reversal, a full characterization of the fragility of dense suspensions is however absent. Here we fill this gap by considering the response to *shear rotations*, i.e. rotations of the stress axes by an arbitrary angle θ about the gradient direction. We perform shear rotations in experiments, with a specifically designed rheometer, discrete element simulations, and the Gillissen-Wilson constitutive model [32, 33]. We report the viscosity drop as a function of θ and strain after rotation γ .

We also unveil a new non-Newtonian phenomenon: following a shear rotation, the shear viscosity orthogonal to the flow direction, η_{32} , is transiently finite, reaching up to 50% of the usual shear viscosity η_{12} . Moreover, we show that the nature of angular dependence of η_{32} depends on ϕ : while at moderate ϕ , η_{32} shows a change of sign in $\theta \in [0, \pi]$, associated to a force resisting shear rotation for small θ values, for the largest ϕ values it keeps a constant sign. We show that this is due to the decreasing relative contribution of hydrodynamic stresses versus contact stresses when ϕ increases.

Experimental setup We designed a *cross rheometer*, sketched in Fig. 1, made with two parallel plates mounted on two motorized linear stages (Newport MFA-CC) acting in perpendicular directions, allowing for arbitrary relative parallel motion and therefore arbitrary simple shear with velocity gradient orthogonal to the plates. We apply a simple shear (Fig. 1(b)) with velocity gradient $\mathbf{L} = \nabla \mathbf{u} = \dot{\gamma} \mathbf{e}_1 \mathbf{e}_2$ (with $(\nabla \mathbf{u})_{\alpha\beta} = \partial_\beta u_\alpha$), from which we

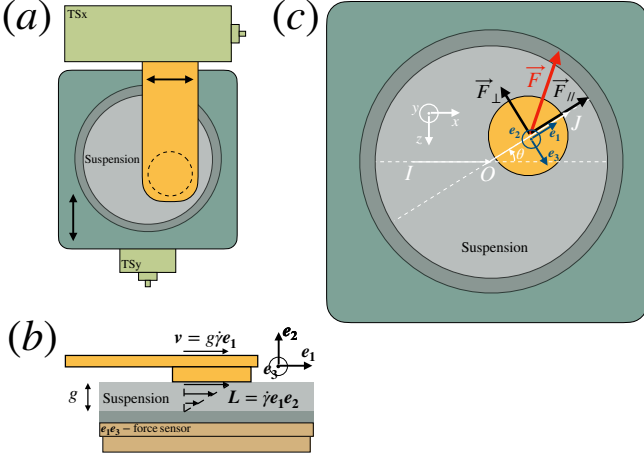


FIG. 1. Sketch of the setup. (a) View along the flow-gradient direction. Two translation stages (light green) independently move an upper plate (orange) and a lower plate (green gray). The suspension (gray) is sheared between these plates. (b) Shear plane view. A force sensor below the lower plate measures the horizontal stresses. (c) Shear rotation by an angle θ in the reference frame of the bottom plate: the top plate moves along IO , then along OJ . A transient force $\mathbf{F} = F_{||}\mathbf{e}_1 + F_{\perp}\mathbf{e}_3$ is recorded during OJ .

define the strain-rate tensor $\mathbf{E} = \dot{\gamma}\hat{\mathbf{E}} \equiv (\mathbf{L} + \mathbf{L}^T)/2$. The shear rate $\dot{\gamma}$ is related to the velocity of the top plane relative to the bottom plane $\mathbf{v} = \dot{\gamma}g\mathbf{e}_1$, $g = 1$ mm being the gap width between the two plates.

A force sensor (AMTI HE6x6-1) measures the tangential force $\vec{F} = \vec{F}_{||} + \vec{F}_{\perp}$ exerted on the lower plate (and thus by the upper plate on the suspension), with $\vec{F}_{||}$ and \vec{F}_{\perp} respectively along \mathbf{e}_1 and \mathbf{e}_3 (Fig. 1(b)-(c)). We define the shear viscosity $\eta_{12} = \boldsymbol{\Sigma} : \mathbf{e}_1\mathbf{e}_2/\dot{\gamma}$, as well as the ‘‘orthogonal’’ shear viscosity $\eta_{32} = \boldsymbol{\Sigma} : \mathbf{e}_3\mathbf{e}_2/\dot{\gamma}$. Both have opposite θ -parities: η_{12} is even, $\eta_{12}(\gamma, \theta) = \eta_{12}(\gamma, -\theta)$, while η_{32} is odd, $\eta_{32}(\gamma, \theta) = -\eta_{32}(\gamma, -\theta)$ (in particular this enforces that $\eta_{32}(\gamma, 0)$ and $\eta_{32}(\gamma, \pi)$ vanish).

A shear rotation is a preshear (IO on Fig. 1(c)) of 10 strain units, a strain large enough to reach steady state, followed by a second shear where we rotate the flow direction \mathbf{e}_1 and vorticity direction \mathbf{e}_3 by an angle $\theta \in [0, 2\pi]$ around the gradient direction \mathbf{e}_2 (OJ in Fig. 1(c)). The viscosities $\eta_{12}(\gamma, \theta)$ and $\eta_{32}(\gamma, \theta)$ are recorded via a DAQ (USB-1608FS-PLUS, MCCDAQ) as a function of the subsequent strain $\gamma < 10$. The strain resolution is $\sim 3 \times 10^{-3}$ and the lowest available strain is $\sim 1 \times 10^{-2}$, and θ is sampled every $\pi/18$.

The suspension particles are PMMA spheres with a diameter of 40 μm (Microbeads TS40). They are dispersed in PEG (Sigma-Aldrich, $\eta_0 = 38.4$ Pa s) (resp. silicon oil M1000, Roth, $\eta_0 = 0.98$ Pa s) for suspensions at $\phi = 0.45$ (resp. $\phi = 0.57$).

Numerics & model We perform the same protocol in DEM simulations of a suspension of $N = 2000$ frictional particles subject to lubrication and contact forces in a tri-periodic configuration, using a method described in [27, 34]. The suspension is bidisperse (with a size ratio 1 : 1.4) and the friction coefficient is $\mu_p = 0.5$.

We also compare our results to the predictions of the GW model, a model capturing the features of shear reversal [32, 33]. The GW model considers the time evolution of a fabric tensor $\langle \mathbf{nn} \rangle$ where \mathbf{n} is the unit separation vector between pairs of particles in a near interaction via contact or lubrication forces

$$\partial_t \langle \mathbf{nn} \rangle = \mathbf{L} \cdot \langle \mathbf{nn} \rangle + \langle \mathbf{nn} \rangle \cdot \mathbf{L}^T - 2\mathbf{L} : \langle \mathbf{nnnn} \rangle - \beta \left[\mathbf{E}_e : \langle \mathbf{nnnn} \rangle + \frac{\phi}{15} (2\mathbf{E}_c + \text{Tr}(\mathbf{E}_c)\boldsymbol{\delta}) \right], \quad (1)$$

with \mathbf{E}_c (resp. \mathbf{E}_e) the compressive (resp. extensive) part of \mathbf{E} , and β a free parameter. The tensor $\langle \mathbf{nnnn} \rangle$ is approximated in terms of $\langle \mathbf{nn} \rangle$ with the Hinch & Leal closure [35]. Furthermore, the GW model decomposes the stress $\boldsymbol{\Sigma}$ in contributions from hydrodynamics, $\boldsymbol{\Sigma}^H$, and contacts, $\boldsymbol{\Sigma}^C$,

$$\frac{\boldsymbol{\Sigma}^H}{\eta_s \dot{\gamma}} = \alpha \hat{\mathbf{E}} : \langle \mathbf{nnnn} \rangle; \quad \frac{\boldsymbol{\Sigma}^C}{\eta_s \dot{\gamma}} = \chi \hat{\mathbf{E}}_c : \langle \mathbf{nnnn} \rangle. \quad (2)$$

Here $\alpha = \frac{\alpha_0}{(1-\phi/\phi_{\text{RCP}})^2}$ and $\chi = \frac{\chi_0}{(1-\xi/\xi_J)^2}$, with α_0 and χ_0 free parameters, are such that they diverge respectively at the random close packing volume fraction ϕ_{RCP} and when the ‘jamming coordinate’ $\xi = -\frac{\langle \mathbf{nn} \rangle : \mathbf{E}_c}{|\mathbf{E}_c|}$ reaches the the jamming value $\xi_J = \phi_J \frac{(213\beta^2 - 234\beta + 2080)}{15(9\beta^2 + 54\beta + 416)}$ [32, 36], which in steady state occurs at the frictional jamming point, $\phi = \phi_J < \phi_{\text{RCP}}$.

Results In Fig. 2(a), we show the viscosity $\eta_{12}(\gamma, \theta)$ measured in experiments, for a moderately dense suspension at $\phi = 0.45$. It decreases at low strain values, passes via a minimum before increasing back to its steady-state value. The minimum is located at a strain γ_{min} increasing with θ , from $\gamma_{\text{min}} \lesssim 0.1$ for the smallest considered θ values to $\gamma_{\text{min}} \approx 0.35$ for shear reversal ($\theta = \pi$). As shown in Fig. 2(b), the minimum value $\eta_{12, \text{min}}$ gradually decreases when θ increases, to reach its lowest value for shear reversal. Once normalized by the steady-state value η_{12}^{SS} , $\eta_{12, \text{min}}/\eta_{12}^{\text{SS}}$ for a given θ decreases when ϕ increases, as is already known for shear reversal [21]. Interestingly, for the lowest $\phi = 0.45$, $\eta_{12, \text{min}} \approx \eta_{12}^{\text{SS}}$ for $\theta \lesssim \pi/4$: η_{12} seems oblivious to the shear rotation at small angles, which we could interpret as a non-fragile response. (We will see that this is not quite true when considering η_{32} .)

We compare these data with the DEM ones in a radial representation $\eta_{12}(\gamma, \theta)$ in Fig. 2(c), with experiments in the top half and numerics in the bottom half. The agreement is good, besides simulations predicting a quicker relaxation to steady state than actually observed.

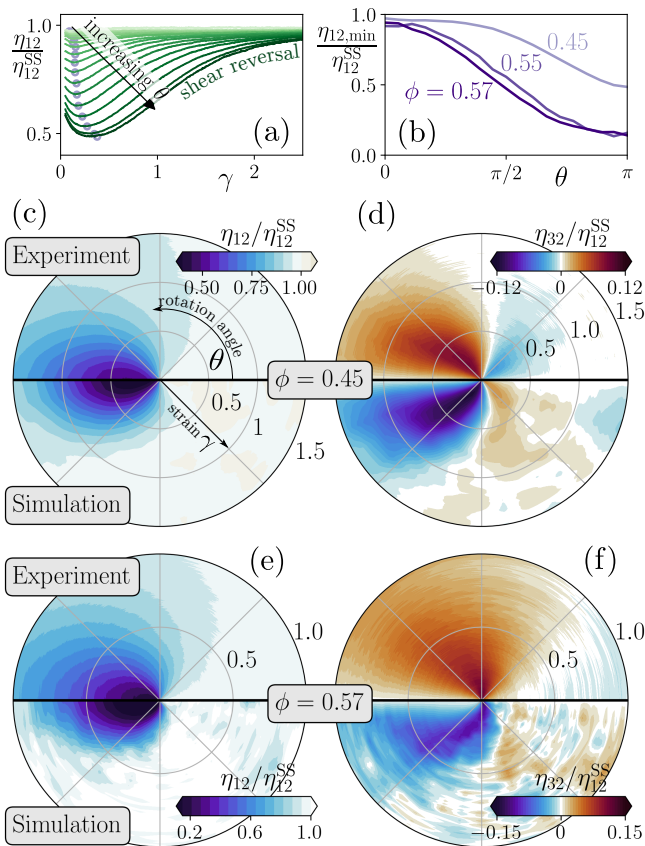


FIG. 2. (a) Shear viscosity η_{12} normalized by the steady-state value η_{12}^{SS} as a function of strain γ in experiments for $\phi = 0.45$, for several values of $\theta \in [0, \pi]$, increasing from light to dark. The minimum values of the viscosity $\eta_{12,\text{min}}/\eta_{12}^{\text{SS}}$ for each θ are circled. (b) $\eta_{12,\text{min}}/\eta_{12}^{\text{SS}}$ as a function of shear rotation angle θ for $\phi = 0.45, 0.55$ and 0.57 . (c) and (d) Polar representation of $\eta_{12}(\gamma, \theta)$ and $\eta_{32}(\gamma, \theta)$, normalized by η_{12}^{SS} , for $\phi = 0.45$, in experiments (top half) and numerical simulations (bottom half). (e) and (f) Same, but for $\phi = 0.57$.

We turn in Fig. 2(d) to η_{32} , again comparing experiments in the top half and numerics in the bottom half. Both data are in excellent agreement and reveal a structure with a mixture of first and second order odd circular harmonics (respectively $\propto \sin\theta$ and $\propto \sin 2\theta$) coming with similar amplitudes. For $0 < \theta \lesssim \pi/2$, we find $\eta_{32} < 0$ for $\gamma \lesssim 1$, i.e. the suspension exerts on the top plate a “restoring” force in the direction of decreasing θ values. In a force control setup where one sets the upper plate force \vec{F}_{\parallel} rather than its displacement, the suspension would thus be stable with respect to shear rotations, by rotating the velocity of the top plate towards lower θ values. By contrast, for $\pi/2 \lesssim \theta < \pi$, we find $\eta_{32} > 0$ for $\gamma \lesssim 2$, which can be interpreted as the suspension tending to bend the top plate trajectory to larger θ values.

In Fig. 2(e),(f), we show η_{12} and η_{32} for $\phi = 0.57$, close to $\phi_J \approx 0.58$. Both experimental and numerical data show

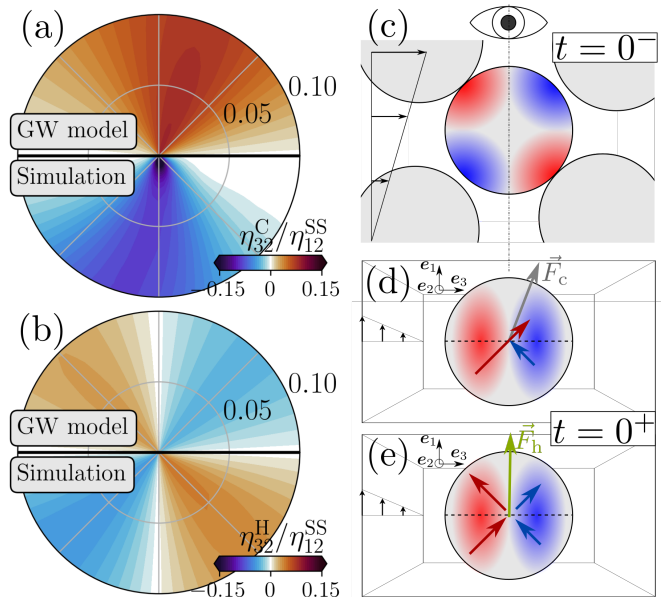


FIG. 3. Contributions to the orthogonal viscosity from contacts (a) and hydrodynamics (b), in the GW model in the top halves and DEM simulations in the bottom halves. (c) A particle during initial shear at $t = 0^-$ has more near contacts in compressional quadrants (red) than elongational quadrants (blue). (d)–(e) Looking down from the gradient direction, just after shear rotation by $\theta = \pi/2$ the new compressional and elongational quadrants are respectively below and above the dashed lines. Contact forces come from the new compressional, and are dominated by the more numerous contacts in the old compressional (red arrow), leading to $\eta_{32}^{\text{C}} > 0$ (d). Hydrodynamic forces have symmetric contributions from new compressional and elongational quadrants, leading to $\eta_{32}^{\text{H}} = 0$ (e).

that the relaxation to steady state is quicker than at $\phi = 0.45$ [21, 23]. More importantly, the first harmonic of η_{32} dominates. For $0 < \theta < \pi$, we find $\eta_{32} > 0$: the suspension always tend to push the top plate to move towards larger θ values, that is, the response is no longer stabilizing for small shear rotations.

Our simulations also show that the stress response is closely mimicked by the microstructure response, characterized by the fabric evolution after shear rotation [34]. Notably, however, the fabric evolution does not exhibit any qualitative change upon increase of ϕ that we could correlate to the change of behavior of η_{32} .

To understand the origin of the η_{32} behavior, we interrogate the GW model, performing shear rotations and looking separately at the contact and hydrodynamic contributions to the stress response. As shown in Fig. 3(b), the large second harmonic of η_{32} is due to the hydrodynamic component η_{32}^{H} , which at $\phi = 0.45$ still accounts for a substantial part of the total stress [28]. In contrast, the contact contribution η_{32}^{C} has a dominant first harmonic, with $\eta_{32}^{\text{C}} > 0$ for $0 < \theta < \pi$, as shown in Fig. 3(a). This is confirmed by numerical simulations,

which compare well to the predictions of the GW model for both stress components.

The difference between contact and hydrodynamic contributions can be qualitatively understood. In Fig. 3(c), we sketch a particle during preshear. It shows a fore-aft asymmetry: it has more near interactions (lubricated and in contact) in the compressional quadrants (in red) than in the elongational one (in blue). The same particle is seen from the gradient direction \mathbf{e}_2 right after a shear rotation with $\theta = \pi/2$ in Fig. 3(d),(e). After rotation, the fore-aft asymmetry accumulated in preshear is a “left-right” asymmetry, and fore-aft symmetry is temporarily restored. Post-rotation contact stresses (Fig. 3(d)) stem from contacts in the post-rotation compressional quadrant, below the dashed line, and due to the left-right asymmetry, are dominated by contacts that carry over from the pre-rotation by the intersect of pre- and post-rotation compressional quadrants. Contact forces \vec{F}_C in this overlap region (red vector) are such that $\mathbf{e}_3 \cdot \vec{F}_C > 0$, giving a positive contribution to η_{32} . By contrast, in Fig. 3(d), all interactions contribute hydrodynamic forces, and the fore-aft symmetry ensures that the hydrodynamic contribution from the post-rotation elongational and compressional quadrants share the same \mathbf{e}_1 component, but have opposite \mathbf{e}_3 component. This results in a net-zero hydrodynamic contribution to η_{32} .

Whereas this reasoning can be extended to show that $\eta_{32}^C > 0$ for $\theta \in]0, \pi[$, the sign of η_{32}^H for $\theta \neq \pi/2$ depends on aspects of the distribution of near interactions that cannot be deduced from symmetry considerations. The GW model however gives us a quantitative picture alongside a microstructural insight. Calling $\langle \mathbf{nn} \rangle^{\text{ss}}$ the steady-state fabric in pre-shear, we get the following contributions to η_{32} at $\gamma = 0^+$ [34]

$$\begin{aligned} \frac{\eta_{32}^H}{\eta_s} &= \frac{\alpha(\phi)}{14} \sin 2\theta (\langle \mathbf{nn} \rangle_{xx}^{\text{ss}} - \langle \mathbf{nn} \rangle_{zz}^{\text{ss}}) \\ \frac{\eta_{32}^C}{\eta_s} &= \frac{\chi(\xi)}{7} \left[\frac{\sin 2\theta}{4} (\langle \mathbf{nn} \rangle_{xx}^{\text{ss}} - \langle \mathbf{nn} \rangle_{zz}^{\text{ss}}) - \sin \theta \langle \mathbf{nn} \rangle_{xy}^{\text{ss}} \right], \end{aligned} \quad (3)$$

with

$$\xi = \left[\cos^2 \theta \langle \mathbf{nn} \rangle_{xx}^{\text{ss}} + \langle \mathbf{nn} \rangle_{yy}^{\text{ss}} + \sin^2 \theta \langle \mathbf{nn} \rangle_{zz}^{\text{ss}} - 2 \cos \theta \langle \mathbf{nn} \rangle_{xy}^{\text{ss}} \right] / 2.$$

For the contact contribution, we find that the first harmonic dominates for the values of ϕ and β investigated. It is such that $\eta_{32}^C > 0$ for $0 < \theta < \pi$. By contrast, the hydrodynamic contribution only has a second harmonic, and dominates the response at angles close to $\theta = 0$ and $\theta = \pi$. Moreover, its sign is not obvious, as it is set by $\langle \mathbf{nn} \rangle_{xx}^{\text{ss}} - \langle \mathbf{nn} \rangle_{zz}^{\text{ss}}$. With the values of β used here, we always find $\langle \mathbf{nn} \rangle_{xx}^{\text{ss}} - \langle \mathbf{nn} \rangle_{zz}^{\text{ss}} < 0$ in the GW model. For small θ values, it therefore “stabilizes” the microstructure, as $\text{sgn} \eta_{32}^H = -\text{sgn} \theta$, so that it provides

a restoring force acting against the rotation of the flow direction. From previous simulations, $\langle \mathbf{nn} \rangle_{xx}^{\text{ss}} - \langle \mathbf{nn} \rangle_{zz}^{\text{ss}}$ is known to be tiny [23]. In our simulations, where we compute $\langle \mathbf{nn} \rangle$ based on particle pairs separated by at most a gap of $\epsilon_c = 0.05$ times the average radius of the pair, we also find $\langle \mathbf{nn} \rangle_{xx}^{\text{ss}} - \langle \mathbf{nn} \rangle_{zz}^{\text{ss}} < 0$, albeit decreasing in amplitude when ϕ increases. Interestingly, the value of $\langle \mathbf{nn} \rangle_{xx}^{\text{ss}} - \langle \mathbf{nn} \rangle_{zz}^{\text{ss}}$ becomes positive for small enough ϵ_c , which highlights how subtle the hydrodynamic stabilization is.

We have shown how to characterize the macro-fragile response of dense suspensions using shear rotations. We performed shear rotations experimentally, numerically, and in a constitutive model, which revealed a rich phenomenology. The shear viscosity exhibits a dip (except at small θ for the smallest ϕ explored here, $\phi = 0.45$) on strain scales of order unity or less, which amplitude increases upon increase of $|\theta|$ or ϕ increase. Remarkably, whereas in steady state symmetry imposes that η_{32} vanishes, we find that $\eta_{32} \neq 0$ during the transient micro-structure reorganization following a shear rotation, with $|\eta_{32}|$ reaching up to 50% of η_{12} at $\phi = 0.57$, and 10% of η_{12}^{SS} . The qualitative angular structure of $\eta_{32}(\gamma, \theta)$ depends on ϕ , which is explained by the predominance of either hydrodynamic or contact stresses. For $\phi = 0.45$, the second harmonic of $\eta(\gamma, \theta)$ is large as hydrodynamic stresses dominate, while for $\phi = 0.57$ it is small as contact stresses dominate. One consequence is that for small θ , η_{32} produces a force that acts to reduce (stabilize) θ at smaller ϕ while it increases (destabilizes) θ at larger ϕ .

These findings are relevant to virtually all actual flows of suspensions that involve changes in the flow geometry, e.g. extrusions, flows of suspensions in porous materials, landslides on varying slope directions. The decrease of η_{12} under shear rotations has already been used to design energy-saving flow strategies [13, 14], however the behavior of η_{32} has so far been overlooked. Whereas in this work we impose the deformation and measure η_{32} , in many cases one imposes the force or stress. A finite η_{32} may lead to non-trivial trajectories, e.g. during the pulling or the sedimentation of an object in a dense suspension, especially if the suspension is not stable against shear rotations.

We have here focused on shear rotations, which form only a subset of all the flow changes that can happen in a complex geometry. In general one would also need to characterize changes from simple shear to extensional flows, and of course non-uniform flows, which are known to induce migration phenomena [37]. While characterizing all flow histories relevant for applications (or even a carefully selected subset) is a major task, our results show that it would certainly reveal non-trivial yet possibly important stress responses. As the GW model captures the salient features of the stress response under shear rotation, as well as for non-uniform flows [38], it

could also prove an efficient design tool in this endeavour.

Acknowledgements. Work funded in part by the European Research Council under the Horizon 2020 Programme, ERC grant agreement number 740269.

-
- [1] M. M. Denn and J. F. Morris, Annual Review of Chemical and Biomolecular Engineering **5**, 203 (2014).
- [2] C. Ness, R. Seto, and R. Mari, Annual Review of Condensed Matter Physics **13**, 97 (2022).
- [3] G. Ovarlez, F. Bertrand, and S. Rodts, Journal of Rheology (1978-present) **50**, 259 (2006).
- [4] F. Boyer, E. Guazzelli, and O. Pouliquen, Physical Review Letters **107**, 188301 (2011).
- [5] I. E. Zarraga, D. A. Hill, and D. T. L. Jr, Journal of Rheology (1978-present) **44**, 185 (2000).
- [6] S.-C. Dai, E. Bertevas, F. Qi, and R. I. Tanner, Journal of Rheology (1978-present) **57**, 493 (2013).
- [7] T. Dbouk, L. Lobry, and E. Lemaire, Journal of Fluid Mechanics **715**, 239 (2013).
- [8] A. Vázquez-Quesada, R. I. Tanner, and M. Ellero, Physical Review Letters **117**, 108001 (2016).
- [9] L. Lobry, E. Lemaire, F. Blanc, S. Gallier, and F. Peters, Journal of Fluid Mechanics **860**, 682 (2019).
- [10] R. Seto, R. Mari, J. F. Morris, and M. M. Denn, Physical Review Letters **111**, 218301 (2013).
- [11] M. Wyart and M. E. Cates, Physical Review Letters **112**, 098302 (2014).
- [12] F. Blanc, E. Lemaire, and F. Peters, Journal of Fluid Mechanics **746**, 10.1017/jfm.2014.160 (2014).
- [13] N. Y. C. Lin, C. Ness, M. E. Cates, J. Sun, and I. Cohen, Proceedings of the National Academy of Sciences **113**, 10774 (2016).
- [14] C. Ness, R. Mari, and M. E. Cates, Science Advances **4**, eaar3296 (2018).
- [15] M. Ramaswamy, I. Griniasty, J. P. Sethna, B. Chakraborty, and I. Cohen, Incorporating tunability into a universal scaling framework for shear thickening (2022), arXiv:2205.02184 [cond-mat].
- [16] F. Gadala-Maria and A. Acrivos, Journal of Rheology **24**, 799 (1980), publisher: The Society of Rheology.
- [17] T. Narumi, H. See, Y. Honma, T. Hasegawa, T. Takahashi, and N. Phan-Thien, Journal of Rheology (1978-present) **46**, 295 (2002).
- [18] V. G. Kolli, E. J. Pollauf, and F. Gadala-Maria, Journal of Rheology (1978-present) **46**, 321 (2002).
- [19] F. Blanc, F. Peters, and E. Lemaire, Journal of Rheology (1978-present) **55**, 835 (2011).
- [20] N. Y. C. Lin, B. M. Guy, M. Hermes, C. Ness, J. Sun, W. C. K. Poon, and I. Cohen, Physical Review Letters **115**, 228304 (2015).
- [21] F. Peters, G. Giovanni, S. Gallier, F. Blanc, E. Lemaire, and L. Lobry, Journal of Rheology **60**, 715 (2016).
- [22] C. Ness and J. Sun, Physical Review E **93**, 012604 (2016).
- [23] R. N. Chacko, R. Mari, S. M. Fielding, and M. E. Cates, Journal of Fluid Mechanics **847**, 700 (2018).
- [24] D. Lootens, H. van Damme, Y. Hémar, and P. Hébraud, Physical Review Letters **95**, 268302 (2005).
- [25] F. Blanc, F. Peters, and E. Lemaire, Physical Review Letters **107**, 208302 (2011).
- [26] F. Blanc, E. Lemaire, A. Meunier, and F. Peters, Journal of Rheology (1978-present) **57**, 273 (2013).
- [27] R. Mari, R. Seto, J. F. Morris, and M. M. Denn, Journal of Rheology (1978-present) **58**, 1693 (2014).
- [28] S. Gallier, E. Lemaire, F. Peters, and L. Lobry, Journal of Fluid Mechanics **757**, 514 (2014).
- [29] B. M. Guy, M. Hermes, and W. C. K. Poon, Physical Review Letters **115**, 088304 (2015).
- [30] M. E. Cates, J. P. Wittmer, J.-P. Bouchaud, and P. Claudin, Physical Review Letters **81**, 1841 (1998).
- [31] R. Seto, A. Singh, B. Chakraborty, M. M. Denn, and J. F. Morris, Granular Matter **21**, 82 (2019).
- [32] J. J. J. Gillissen and H. J. Wilson, Physical Review E **98**, 033119 (2018).
- [33] J. J. J. Gillissen, C. Ness, J. D. Peterson, H. J. Wilson, and M. E. Cates, Journal of Rheology **64**, 353 (2020), publisher: The Society of Rheology.
- [34] See Supplemental Material at [URL will be inserted by publisher].
- [35] E. J. Hinch and L. G. Leal, J. Fluid Mech. **76**, 187 (1976).
- [36] J. J. J. Gillissen, C. Ness, J. D. Peterson, H. J. Wilson, and M. E. Cates, Physical Review Letters **123**, 214504 (2019).
- [37] É. Guazzelli and O. Pouliquen, Journal of Fluid Mechanics **852**, P1 (2018).
- [38] J. J. J. Gillissen and C. Ness, Physical Review Letters **125**, 184503 (2020).